Evaluation of resonances: adaptivity and AAA rational approximation of randomly scalarized boundary integral resolvents

Oscar P. Bruno[*]   Manuel A. Santana[*]   Lloyd N. Trefethen[†]

Abstract

This paper presents a novel algorithm, based on use of rational approximants of a randomly scalarized boundary integral resolvent in conjunction with an adaptive search strategy and an exponentially convergent secant-method termination stage, for the evaluation of acoustic and electromagnetic resonances in open and closed cavities; for simplicity we restrict treatment to cavities in two-dimensional space. The desired cavity resonances (also known as "eigenvalues" for interior problems, and "scattering poles" or "complex eigenvalues" for exterior and open-cavity problems) are obtained as the poles of associated rational approximants; both the approximants and their poles are obtained by means of the recently introduced AAA rational-approximation algorithm. In fact, the proposed resonance-search method applies to any nonlinear eigenvalue problem associated with a given function $F : U \to \mathbb{C}^{d \times d}$, wherein, denoting $F(k) = F_k$, a complex value k is sought for which $F_k w = 0$ for some nonzero $w \in \mathbb{C}^d$. For the scattering problems considered in this paper, which include interior, exterior and open cavity problems, F_k is taken to equal a spectrally discretized version of a Green function-based boundary integral operator at spatial frequency k. In all cases, the scalarized resolvent is given by an expression of the form $u^* F_k^{-1} v$, where $u, v \in \mathbb{C}^d$ are fixed random vectors. The proposed adaptive search strategy relies on use of a rectangular subdivision of the resonance search domain which is locally refined to ensure that all resonances in the domain are captured. The approach works equally well in the case in which the search domain is a one-dimensional set, such as, e.g., an interval of the real line, in which case the rectangles used degenerate into subintervals of the search domain. A variety of numerical results are presented, including comparisons with well-known methods based on complex contour integration, and a discussion of the asymptotics that result as open cavities approach closed cavities—in all, demonstrating the accuracy provided by the method, for low- and high-frequency states alike.

1 Introduction

We are concerned with the problem of evaluation of resonances supported by open and closed cavities and other scattering structures, which are obtained as solution pairs (u, k) of the eigenvalue problem

$$\Delta u + k^2 u = 0 \tag{1}$$

with eigenfunction u and eigenvalue $-k^2$, posed on an interior or exterior domain Ω, with homogeneous boundary conditions of e.g. Dirichlet, Neumann, or other types. Once approximated by discretized versions of the problem's boundary integral operators (which is done in this paper on the basis of the open- and closed-curve integral equation algorithms of [9,14,23], see also [10]), the resonance-search problem is reduced to the solution of a related Nonlinear Eigenvalue Problem (NEP) for a certain function $F : U \to \mathbb{C}^{d \times d}$, wherein, denoting $F(k) = F_k$, a complex value k is sought for which

$$F_k w = 0 \quad \text{for some nonzero} \quad w \in \mathbb{C}^d. \tag{2}$$

---

[*]Computing and Mathematical Sciences, California Institute of Technology, Pasadena, CA, 91125 USA, obruno@caltech.edu, msantana@caltech.edu

[†]School of Engineering and Applied Sciences, Harvard University, Cambridge, MA 02138 USA (trefethen@seas.harvard.edu)

This contribution focuses on scattering problems, for which the function F in (2) provides a discrete approximation of the associated boundary-integral operator. However the method is general and, indeed, other NEPs unrelated to boundary integral operators are considered in this paper as well.

The proposed approach seeks the desired resonant values k, for which (2) holds, as poles of the randomly scalarized resolvent

$$S(k) = u^* F_k^{-1} v, \quad \text{where} \quad u, v \in \mathbb{C}^d \quad \text{are fixed random vectors.} \tag{3}$$

The desired resolvent poles are obtained as poles of rational approximants of (3); both the rational approximants and their poles are produced numerically by means of the recently introduced AAA rational-approximation algorithm [28]. The proposed eigensolver additionally incorporates an adaptive search strategy and a secant-method termination stage. The adaptive search strategy relies on use of a rectangular subdivision of the resonance search domain which is locally refined to ensure that all resonances in the domain are captured. The adaptivity approach works equally well in the case in which the search domain is a one-dimensional set, such as, e.g., an interval of the real line, in which case the rectangles used degenerate into subintervals of the search domain. The secant-method termination stage, in turn, is an important element in the proposed algorithm, which enables (i) Exponentially fast convergence to near machine precision accuracy starting from AAA-based results of lower accuracy; (ii) Reliable error estimation; and, (iii) A capability to reliably screen the spurious eigenvalues that can (rarely) be produced by the AAA algorithm. In all, the overall proposed approach is simple, easy to implement and rapidly convergent, and it requires limited computation besides the embarrassingly parallelizable evaluation of the scalarized resolvent at various wavenumbers k. A variety of numerical results presented in this paper demonstrate the character of the proposed approach: the method yields highly accurate approximations of scattering resonances and solutions of other NEPs, even in cases involving high frequencies.

A significant literature has developed in recent years in connection with the solution of NEPs. As discussed in the survey article [19], solution methods include root finding methods, contour integration methods, and methods based on linearization of F_k, all of which have been applied to the computation of resonances [2,3,16,27,31,34]. In turn, a set of methods for the NEP that, like the present paper, rely on use of AAA rational approximation, have recently been developed [17,18,22], and specifically, the contributions [17, 18] apply the AAA algorithm to the scalarized resolvent (3). But in these contributions the AAA algorithm is applied in a manner different to the one we use: in those contexts a rational approximation is employed to produce a linearization of F_k whose eigenvalues approximate the desired eigenvalues, whereas the present paper directly uses the poles of the rational approximant of S as approximants of the desired eigenvalues. Closer to our work is the AAA-based algorithm introduced in [7], which considers the transmission of plane waves by a periodic dieletric system. In that approach, numerical solutions of the transmission problem are obtained by means of the finite element method and from such solutions the rational approximant of the coefficient of transmission across the structure is produced—whose poles near the real axis are indicative of the resonant character of the structure, in that they incorporate information concerning some of the structure's complex eigenvalues.

In view of the strengths of the various algorithmic components it incorporates, the proposed algorithm is flexible, accurate and efficient. The algorithm's use of rational approximations allows for utilization of scalarized-resolvent data points on arbitrary sets of frequencies, enabling, in particular, the use of arbitrarily distributed data points on the boundaries of rectangles—which greatly facilitates the design of the adaptive strategy proposed in this paper. Further, use of simple intervals of the real line suffices for evaluation of real eigenvalues. The secant-method termination stage, finally, provides significant benefits concerning accuracy and reliability, as mentioned in points (i)-(iii) above.

This paper is organized as follows. Sections 2 and 3 review the integral-equation and associated numerical schemes used in this paper to represent solutions of the Helmholtz equation (1) for open and closed two-dimensional domains. Section 4 provides a brief description of the AAA algorithm. The overall

proposed approach for the solution of NEPs is then described in Section 5. A variety of numerical results presented in Section 6 include NEPs unrelated to Laplace eigenvalues, comparisons with well-known methods based on complex contour integration, illustrations concerning low- and high-frequency Laplace eigenvalue problems for open and closed cavities, as well as the asymptotics that result as open cavities approach closed cavities—in all, demonstrating the accuracy provided by the method even for low- and high-frequency states alike.

2 Eigenvalue problems, Green Functions and Integral Operators

We consider eigenvalue problems of the form (1), posed in open two dimensional spatial domains Ω with smooth boundaries Γ, and with homogeneous boundary conditions on Γ. Three types of spatial domains are considered in this paper, namely, domains Ω equal to: (a) The complement Γ^c of an open arc Γ in $\mathbb{R}^2$; (b) The region interior to a closed curve Γ in $\mathbb{R}^2$; and, (c) The region exterior to a closed curve Γ in $\mathbb{R}^2$. For definiteness this paper mostly concerns eigenvalue problems under homogeneous Dirichlet boundary conditions

$$u|_\Gamma = 0 \tag{4}$$

for each of these domain-types. Homogeneous Neumann and Zaremba boundary conditions can be handled similarly [1, 2, 23]; in fact, results of Neumann problems produced by the proposed algorithm are briefly mentioned in Section 6.4.

Our treatment of the problem (1)–(4) is based on use of the two dimensional Helmholtz Green function $G_k(x,y) := \frac{i}{4}H_0^1(k|x-y|)$ (where H_0^1 denotes the Hankel function of the first kind of order 0) and the associated single-layer potential representation

$$u(x) = \int_\Gamma G_k(x,y)\psi(y)\, ds_y, \quad x \in \Omega, \tag{5}$$

of the eigenfunction u in terms of a surface density ψ. In view of the well known [13, 25] continuity of the single layer potential $u = u(x)$ as a function of $x \in \mathbb{R}^2$, up to and including Γ, we consider the boundary integral operator $F_k : H^{-1/2}(\Gamma) \to H^{1/2}(\Gamma)$ (resp. $F_k : \widetilde{H}^{-1/2}(\Gamma) \to H^{1/2}(\Gamma)$) given by the expression

$$F_k[\psi](x) = \int_\Gamma G_k(x,y)\psi(y)ds_y, \quad x \in \Gamma \tag{6}$$

on a closed (resp. open) smooth curve Γ. See [25] and [23] and references therein for detailed definitions of the Sobolev spaces $H^{\pm 1/2}$ and $\widetilde{H}^{1/2}$ relevant to the closed and open-arc single layer operators, respectively.

As suggested above, the k-dependent operator (6) can be used to tackle the interior, exterior and open-arc eigenvalue problems under consideration. Indeed, for any smooth open arc or closed curve Γ and for any given density function ψ defined on Γ, we have [25] (i) The function u given by the representation formula (5) is a solution of equation (1) for all $x \in \Gamma^c$; and, (ii) The function $u \neq 0$ satisfies the Dirichlet boundary condition (4) if and only if $\psi \neq 0$ is a solution of the equation $F_k[\psi] = 0$. It can accordingly be shown that the resolvent operator $(F_k)^{-1}$ is an analytic function of k for $\Im k > 0$, and that that given a complex number $k = \mu$ with $\Im \mu \leq 0$, the number $-\mu^2$ is an eigenvalue of the problem (1)–(4) if and only if the value $k = \mu$ is a pole of the resolvent operator $(F_k)^{-1}$ as a function of k. This fact is established in [32, Prop. 7.10] for closed-curve interior problems (for which μ in the lower half-plane $\Im \mu \leq 0$ must actually be real) and for closed-curve exterior problems (for which μ must satisfy $\Im \mu < 0$). As indicated in what follows, the corresponding result for open-arc problems can be established along lines similar to those in [32, Prop. 7.10].

A critical element in the extension of these results to the open-arc case is the injectivity of the mapping $\psi \to u$, which, according to equation (5), maps functions defined on Γ to functions defined in $\mathbb{R}^2$. The corresponding closed-curve injectivity result for the exterior problem is established in [32] by showing that

3

if ψ satisfies the equation $F_k(\psi) = 0$, then the associated function u given by (5) is a Laplace eigenfunction in the interior of Γ and that, therefore, the corresponding eigenvalue $-\mu^2$ must be real, and by subsequently making use of the jump relations for the single- and double-layer potentials across Γ. The corresponding closed-curve result for the interior problem is established similarly. For the open-arc problem we have no equivalent of the interior region, but the injectivity result can be established nevertheless, simply by using the jump relation for the normal derivative of the single-layer potential. The equivalence between Laplace eigenvalues $-\mu^2$ with μ in the lower half-plane and poles $k = \mu$ of the resolvent $(F_k)^{-1}$ then follows for the open arc case in a manner analogous to that put forth in [32, Sec. 7] by relying on the second-kind formulation for open problems introduced in [9, 23].

In sum, noting that, without loss of generality, the search for values of k satisfying the eigenvalue problem (1)–(4) may be restricted to the lower half-plane $\Im k \leq 0$, the eigenvalues may be sought as real poles $k = \mu$ of the resolvent operator $(F_k)^{-1}$ for the eigenvalue problem in the interior of a closed curve Γ, and as complex poles $k = \mu$ of the same operator, with $\Im \mu < 0$, for either the eigenvalue problem in the exterior of a closed curve Γ or for the complement of an open arc Γ. The associated eigenfunctions u then result via equation (5) with density (or, for multiple eigenvalues, densities) ψ in the nullspace of the operator F_k. In other words, the integral equation setting just described reduces the eigenvalue problem (1)–(4) for interior and exterior closed-curve and open arc problems to an NEP for the single-layer operator (6) with values of k restricted to the lower half-plane.

3 Numerical Instantiation of the Integral Operator F_k

The numerical implementations utilized in this paper for the Green function-based integral operator (6) are based on the discretization methods presented in [14, Sec. 3.6] (resp. [9, Secs. 3.2, 5.1]) for closed (resp. open) curves in the plane. For simplicity, our computational examples restrict attention to smooth curves Γ and boundary conditions of Dirichlet type, although related methods are available [1, 9, 14] that enable corresponding treatments for non-smooth boundaries [1, 14] as well as Neumann, Robin and Zaremba boundary conditions [1, 9]. As indicated in [9], in particular, the numerical implementation of the integral operator (6) for open arcs Γ requires consideration of the edge singularities that are incurred by the solutions ψ of problems of the form $F_k[\psi] = f$ even for functions f defined on Γ which do not contain such singularities.

For both open- and closed-curve problems the methods [9, 14] discretize the single layer operator F_k on the basis of Nyström-type methodologies—utilizing a sequence of points along the curve Γ for both integration and enforcement of the equation. For closed curves Γ the discretization is produced as the image under the curve parametrization of a uniform grid in the parameter interval $[0, 2\pi]$; in the case of open curves the discretization results as the image of a Chebyshev mesh in the parameter interval $[-1, 1]$. In both cases the unknown functions ψ are expressed in terms of Fourier-based expansions in the parameter intervals, which are then integrated termwise by reducing each integrated term to evaluation of explicit integrals. The edge singularities of the function ψ in the open-arc case are tackled by explicitly factoring out the singular term: using a smooth parametrization $\mathbf{r} = \mathbf{r}(t)$ of the open curve Γ ($-1 \leq t \leq 1$) and writing $\psi(\mathbf{r}(t)) = \phi(\mathbf{r}(t))/\sqrt{1 - t^2}$, it follows that ϕ is a smooth function. Upon introduction of a cosine change of integration variables two desirable effects occur, namely, the function ϕ is converted into a periodic and even function which may be expanded in a cosine series with high accuracy, and, at the same time, the square root term in the denominator is cancelled by the Jacobian of the change of variables. The method is completed by exploiting explicit expressions for the integral of products of a logarithmic kernel and the cosine Fourier basis functions. As illustrated in [9] and other contributions mentioned above, these methodologies can produce scattering solutions with accuracies near machine precision on the basis of relatively coarse discretizations, even for configurations involving high spatial frequencies.

In particular, these procedures produce highly accurate numerical approximations of the integral operator F_k in (5)—which we exploit in the context of this paper to produce accurate numerical evaluations

of eigenvalues and eigenfunctions. As indicated in Section 5, the poles of (a randomly scalarized version of) this integral operator, which, per the discussion in Section 2, correspond to Laplace eigenvalues in the various cases considered, are then obtained as poles of associated AAA rational approximants. The corresponding eigenfunctions are obtained via consideration of a Gaussian elimination-based de-singularization procedure described in Section 5. For added accuracy, the methods in that section propose two alternatives, namely, the use of either iterated AAA rational approximants on one hand, or application of the secant method after an initial evaluation of poles via the AAA approach, on the other hand. In practice we have observed that, without exceptions, accuracies near machine precision are obtained for both eigenvalues and eigenfunctions on the basis of the overall proposed methodology; a few related illustrations are presented in Section 6.

4 Rational Approximants and the AAA Algorithm

The AAA algorithm is a greedy procedure for the construction of a rational approximant to a given complex-valued function f on the basis of its values on an N-point set $Z_N \subset \mathbb{C}$ (full details can be found in [28]). Given the set $\{(z, f(z)) \mid z \in Z_N\}$, the algorithm proceeds by selecting a sequence of points $z_j \in Z_N$, starting with some point z_1, which in principle can selected arbitrarily, but which the Matlab implementation [15] takes as a $z \in Z_N$ for which the function value $f(z)$ is farthest from the mean of the set $\{f(z) \mid z \in Z_N\}$. The remaining points are then selected inductively. Once points $z_j \in Z_N$ ($1 \leq j \leq m$) have been chosen, with corresponding function values $f_j \equiv f(z_j)$, for a suitably chosen vector $w^m = (w_1^m, \ldots, w_m^m)$ of complex weights w_j^m satisfying $\sum |w_j|^2 = 1$, the procedure to obtain z_{m+1} starts by constructing the barycentric-form rational function

$$r(z) = \frac{n^m(z)}{d^m(z)} = \sum_{j=1}^m \frac{w_j^m f_j}{z - z_j} \bigg/ \sum_{j=1}^m \frac{w_j^m}{z - z_j}, \tag{7}$$

where, as suggested by the notation used, $n^m(z)$ and $d^m(z)$ denote the numerator and denominator in the right-hand expression in (7). The vector w^m is selected as follows: calling $A_m = \{(\widetilde{w}_1, \ldots, \widetilde{w}_m) \in \mathbb{C}^m \mid \sum |\widetilde{w}_j|^2 = 1\}$, w^m is defined as a minimizer of the least-squares problem

$$w^m = \arg\min_{\widetilde{w} \in A_m} \sum_{z \in Z_N^m} |f(z) d_{\widetilde{w}}(z) - n_{\widetilde{w}}(z)|^2,$$

where $Z_N^m = Z_N \setminus \{z_j \mid j = 1, \ldots, m\}$, $n_{\widetilde{w}}(z) = \sum_{j=1}^m \frac{\widetilde{w}_j f_j}{z - z_j}$ and $d_{\widetilde{w}}(z) = \sum_{j=1}^m \frac{\widetilde{w}_j}{z - z_j}$. Once the minimizer w^m has been computed, z_{m+1} is defined as a point $z \in Z_N^m$ for which $|f(z) - n^m(z)/d^m(z)|$ is maximum relative to $\max\{f(z) \mid z \in Z_N\}$. The algorithm terminates when this maximum is less than or equal to a specified tolerance, and the last rational function (7) obtained as part of the z_j selection process provides the desired rational approximant.

All of the numerical illustrations presented in this paper utilize the AAA implementation included with Chebfun [15].

5 Solution of NEPs

The discussion in Sections 2 and 3 reduces the eigenvalue problem (1)–(4) to NEPs for the single-layer operator (6) (and the corresponding discrete approximate operator introduced in Section 3), with values of k restricted to the lower half-plane. This section presents numerical algorithms for the solution of this NEP and, indeed, of general NEPs for which the resolvent operator $(F_k)^{-1}$ is a meromorphic function of k.

As indicated in Section 1, the proposed NEP algorithm obtains the eigenvalues k as the poles of a AAA rational approximant associated with the randomly scalarized resolvent $S(k)$ in equation (3). While, in

principle, values of the scalarized resolvent $S(k)$ on any given subset of the complex plane may be used to obtain eigenvalues, throughout this paper we restrict attention to algorithms based on use of values $S(k)$ for k on a given curve $\mathcal{C}$ in the complex plane. Both open and closed curves $\mathcal{C}$ may be used, such as e.g. the closed curves equal to the boundaries of either a rectangle or a circle, or the open curve equal to an interval $[a, b]$ contained in the real axis. Proceeding on the basis of such data, Algorithm 1 below evaluates either eigenvalues contained on the union $\widetilde{\mathcal{C}}$ of $\mathcal{C}$ and its interior, if $\mathcal{C}$ is a closed curve, or eigenvalues along the curve $\mathcal{C}$, if $\mathcal{C}$ is an open curve. Algorithm 2, in turn, seeks to find all such eigenvalues, namely, all eigenvalues contained within $\widetilde{\mathcal{C}}$ if $\mathcal{C}$ is a closed curve, and all eigenvalues along $\mathcal{C}$ if $\mathcal{C}$ is an open curve.

Algorithm 1: Basic Algorithm

---

1 Select a set $Z_N = \{k_1, \ldots, k_N\}$ which is a subset of an open curve $\mathcal{C}$ or a closed curve and its interior $\tilde{\mathcal{C}}$

2 Choose random vectors $u, v \in \mathbb{C}^d$

3 for $j = 1, \ldots, N$ **do**

4 $\quad$ $s_j = u^* F(k_j)^{-1} v$

5 end

6 Compute a rational approximant $r(z)$ associated with the set $\{(k_j, s_j) \mid s_j = S(k_j), j = 1, \ldots, N\}$ using the AAA algorithm

7 Return the poles of $r(z)$ in $\mathcal{C}$ or $\tilde{\mathcal{C}}$

In detail, the pseudo-code Algorithm 1 proceeds by first evaluating the scalarized resolvent $S = S(k)$ at a suitably selected set $Z_N = \{k_1, \ldots, k_N\}$ of points along $\mathcal{C}$ to obtain the set $G_N = \{(k_j, s_j) \mid s_j = S(k_j), \ j = 1, \ldots, N\}$. Using this set of pairs Algorithm 1 then obtains a rational approximant $r = r(k)$ by means of the AAA algorithm, and, for a closed curve $\mathcal{C}$, the poles of $r(k)$ contained in $\widetilde{\mathcal{C}}$ (resp. for an open curve $\mathcal{C}$, the poles on or sufficiently close to $\mathcal{C}$) are returned as approximations of eigenvalues of F_k.

Algorithm 2: Adaptive Algorithm

Input: A set **C** which is either a rectangular region $\widetilde{\mathcal{C}}$ or real interval $\mathcal{C}$ and eigenvalues e from Algorithm 1 applied to **C**

1 Function `eigadaptive(`e`, `C`)`

2 $\quad$ Partition **C** dyadically in each dimension into sets C_i

3 $\quad$ **for** *each C_i* **do**

4 $\quad\quad$ Compute n_i, the number of eigenvalues e in C_i

5 $\quad\quad$ Compute eigenvalues $\widetilde{e}$ from Algorithm 1 applied to C_i

6 $\quad\quad$ Compute $\widetilde{n}_i$, the number of eigenvalues $\widetilde{e}$ inside C_i

7 $\quad\quad$ **if** $n_i = \widetilde{n}_i$ **then**

8 $\quad\quad\quad$ **return** $\widetilde{e}$

9 $\quad\quad$ **else**

10 $\quad\quad\quad$ **return** `eigadaptive(`$\widetilde{e}$`, `C_i`)`

11 $\quad$ **end**

Typically Algorithm 1 finds all of the eigenvalues within $\mathcal{C}$ or $\widetilde{\mathcal{C}}$, as relevant, provided the number of such eigenvalues is not too large. This observation suggests the development of an adaptive version of Algorithm 1, which, as detailed in the pseudo-code titled Algorithm 2, is specialized to searches for eigenvalues within either (i) A rectangular region $\widetilde{\mathcal{C}}$, or, (ii) A real interval $\mathcal{C} = [a, b]$. The algorithm proceeds by finding all eigenvalues within $\mathcal{C}$ or $\widetilde{\mathcal{C}}$, and then reapplying Algorithm 1 upon recursive dyadic subdivision along each dimension. The recursion ends when the number of poles obtained does not change upon subdivision. Clearly, the fact that Algorithm 1 is applicable to arbitrary curves is highly beneficial

in this context, as the use of rectangular regions lends itself for the adaptive subdivision strategy used in Algorithm 2.

It is important to note that the AAA algorithm may fail to accurately produce the eigenvalues within $\mathcal{C}$ or $\widetilde{\mathcal{C}}$ if the set G_N does not adequately represent $S(k)$ along the curve $\mathcal{C}$. An inadequate representation generally manifests itself through the appearance of false poles (see [28]) near $\mathcal{C}$, which in practice may be detected via a convergence analysis as points are added to the set G_N and N grows accordingly. Without exception, in practice we have found that, provided the curve $\mathcal{C}$ encloses a sufficiently small number of eigenvalues, once convergence to a fixed set of poles has occurred, the poles found within $\mathcal{C}$ or $\widetilde{\mathcal{C}}$ correspond in a one-to-one fashion to all the eigenvalues in that region. Starting from such poles, eigenvalues with near machine precision accuracy can be obtained by means of one of two possible methods, namely (i) Use of a subsequent "localized" AAA approximation applied to a few points around each eigenvalue obtained in the initial application of AAA; or, (ii) Use of the secant method applied to $1/S(k) = 1/(u^* F_k^{-1} v)$ starting at each one of the eigenvalues obtained in the initial application of AAA. In regard to method (i), we have found that use of localized AAA approximations over a circle of radius $\rho_{\mathrm{conv}} = 10^{-5}$ works well in many cases, but generally tuning of the parameter ρ_{conv} is necessary for convergence and, indeed, it is difficult in practice to determine whether convergence to a given tolerance has occurred, except in test cases for which the eigenvalues are known beforehand. Fortunately, method (ii) does not present this difficulty and, as it happens, it provides an additional significant advantage. Indeed, in practice we have found that, without exception, use of method (ii) results in convergence to an eigenvalue, and, clearly, the convergence history provides an error estimate for the eigenvalue found—and we thus recommend this approach as a completion procedure for each eigenvalue found. The numerical examples in Section 6 illustrate the performance of Algorithm 2 augmented by means of each one of these localized accuracy-improvement procedures.

Eigenvectors corresponding to each eigenvalue can finally be obtained via evaluation, based on Gaussian elimination, of the nullspace of the matrix F_k at each eigenvalues k obtained. In detail, using Gaussian elimination with pivoting leads to an LU decomposition of the form $F_k = LU$. Using this decomposition the nullspace of F_k can be computed by a simple two-step procedure consisting of (i) Selection of a set of canonical-basis vectors that are mapped to zero by the rows in the matrix U that are associated with the nonzero pivots; and, (ii) For each zero pivot in the matrix U, construction and solution of the reduced systems that result from the elimination of the rows and columns in U containing the zero pivots, and with right-hand sides equal to the negatives of each of the eliminated columns but excluding the column element in the eliminated row. Null vectors could also be computed by means of the singular value decomposition for sufficiently small problems such as the two dimensional examples considered in this paper, but the singular value decomposition method would be problematic for larger problems such as those arising from scattering in three dimensions, whereas, in view of [30], GMRES-based iterative methods related to the LU-based approach mentioned above can be envisioned. An alternative considered in [7, Sec. 2.2] produces eigenvectors on the basis of the rational approximation itself, albeit, according to our experiments, at the expense of some loss of accuracy. In this contribution the aforementioned Gaussian elimination procedure is used, as it requires no additional approximation after application of the secant based refinement method, and as it results in accuracies comparable to those enjoyed by the eigenvalues themselves.

6   Numerical Examples

A few numerical illustrations of the proposed methodology are presented in what follows, including a demonstration of the performance of Algorithm 2 on NEPs unrelated to Laplace eigenvalues (Section 6.1); a set of examples concerning low-frequency Laplace eigenvalues (Section 6.2) and a comparison to complex contour integration methods (Section 6.3); an exploration of the rate at which scattering poles associated with open arcs converge to the corresponding interior eigenvalues as the opening closes (Section 6.4); and finally, a set of examples concerning high-frequency Laplace eigenvalues and eigenfunctions (Section 6.5).

6.1 Adaptivity and exhaustive eigenvalue evaluation

This section illustrates the ability of Algorithm 2 to exhaustively evaluate the set of eigenvalues of a given NEP that are contained in a given region in the complex plane (see also the examples mentioned in the first paragraph of Section 6.5). To do this, two well known problems included in the NLEVP collection [6] are considered, namely, the "CD player problem" and the "Butterfly problem"; the corresponding eigenvalues are purely real in the first case and complex but not real in the second case. The CD player problem is an eigenvalue problem for a 60×60 matrix polynomial of the form $F(k) = k^2 I + k A_1 + A_0$ arising in the study of a CD-player control task [12]. We restrict attention to the interval $[-50, 5]$ on the real axis, within which the problem has 60 eigenvalues with absolute values as small as $2.23e - 4$ and as large as 41.1399; the real-interval version of Algorithm 2 was used with a total number of 300 points k_j along each subinterval. The second problem is the butterfly problem, in which eigenvalues of a 64×64 matrix polynomial $F(k) = \sum_{i=0}^{4} k^i A_i$ are sought. The matrices A_i are Kronecker products of linear combinations of the identity and nilpotent Jordan blocks [26]. We tackle the butterfly problem by employing Algorithm 2 applied initially to the box of side length 4 centered at the origin. This problem has 256 eigenvalues, and 100 values of k were used on each side of the square. Figure 1 displays the results produced by the proposed algorithm: in each case the proposed adaptive algorithm obtains all of the eigenvalues in the prescribed regions of the complex plane.
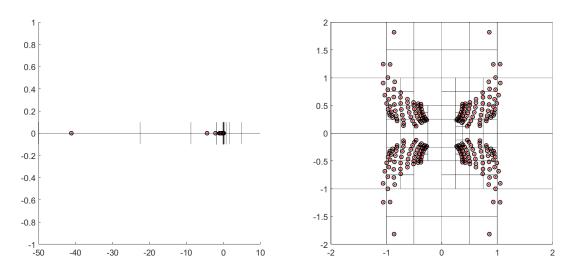

Figure 1: Demonstration of Algorithm 2 on two problems from the NLEVP set [6]. In both panels red points represent exact eigenvalues and black circles represent eigenvalues produced by the proposed numerical method. Black lines represent divisions related to the adaptive version of the algorithm. Left panel: The CD player problem, for which all 60 eigenvalues in the interval $[-50, 5]$ were found to at least 7 digits. Right: The butterfly problem, for which all 256 eigenvalues were found to at least 10 digits. Accuracy near machine precision was subsequently obtained by increasing the discretization in each subregion or by using methods refinement secant- or AAA-based methods described in Sections 5 and 6.2

.

6.2 Low-frequency eigenvalues

This section illustrates the character of the proposed eigensolver in the context of NEPs (2) associated with low-frequency Laplace eigenproblems (1) with boundary conditions (4). Thus, Figures 2 and 3 and Table 1 present Laplace eigenfunctions and eigenvalues for two structures, namely, a (closed) kite-shaped domain and a circular cavity with an aperture of $\pi/8$ radians. All of these eigenvalues and eigenfunctions
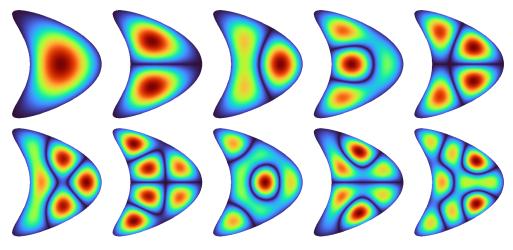
Figure 2: Low-frequency interior eigenvalue problems mentioned in Section 6.2: the first ten interior eigenfunctions for the kite-shaped domain. The associated frequencies k are listed in the left column of Table 1.

were produced by means of Algorithm 2 with an error (evaluated by convergence studies) of the order of $\mathcal{O}(10^{-13})$. In the first case the eigenvalues are real, and they are thus obtained by means of Algorithm 2 with $\mathcal{C}$ equal to an interval in the real axis. In the second case the eigenvalues lie near the real axis; they were obtained using once again Algorithm 2, but, this time using a rectangular curve $\mathcal{C}$ enclosing a finite section of the strip between the real axis and the horizontal line $\Im k = -0.2$; for such a thin strip the localization step was applied by iteratively subdividing the domain along the real axis only.
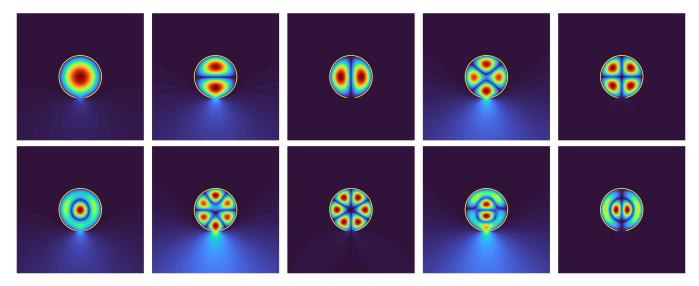

Figure 3: Low-frequency open arc eigenproblems discussed in Section 6.2: the first ten scattering poles of the open circle with imaginary part less than $-0.2i$ (ordered left-to-right and top-to-bottom with increasing values of the real part of the frequency). The associated frequencies k are displayed in the right column of Table 1.

6.3   Comparison with Integral Algorithm 1 in [8] and the block SS method [4]

It is most relevant in the context of this paper to compare the proposed algorithm to other eigensolvers which, like ours, are based on use of Green-function representations. Most often such algorithms rely additionally on complex-contour integration strategies for evaluation of eigenvalues [5, 11, 21, 24, 27, 29, 31,

33, 35], and we therefore select for our comparison the two best-known and prototypical complex-contour eigensolvers, namely, the block SS method [4], and "Integral Algorithm 1" in [8]. To avoid potential confusion with the Algorithm 1 presented in Section 5 above, in what follows we refer to "Integral Algorithm 1" in [8] as "Beyn 1"; for our comparisons we use the implementations of the Beyn 1 and block SS algorithms provided in [19].

Kite	Open Circle
2.209856180349	$2.391850921204 - 0.000866833533i$
3.215653682128	$3.785851440218 - 0.007551333804i$
3.528868275787	$3.831519839558 - 0.000000810935i$
4.303831479675	$5.066410135738 - 0.022753855105i$
4.371112240590	$5.134599571714 - 0.000011845979i$
4.906513621606	$5.486798760828 - 0.010839713761i$
5.291183742145	$6.297659940294 - 0.044691641691i$
5.461743432329	$6.377232306043 - 0.000071959651i$
5.736410337307	$6.923647500434 - 0.056416692369i$
6.172352448525	$7.015195622517 - 0.000013514954i$

Table 1: Computed frequencies k (listed top-to-bottom in this table) such that $-k^2$ is an eigenvalue of the eigenvalue problem (1) corresponding to the eigenfunctions displayed in Figures 2 and 3 (ordered left-to-right and top-to-bottom). All digits listed are believed correct on the basis of numerical convergence analyses.

The block SS method relies on use of matrices containing L columns of random vectors by computing the product

$$U^* F_k^{-1} V \in \mathbb{C}^{L \times L}, \quad \text{where} \quad U, V \in \mathbb{C}^{d \times L} \quad \text{are matrices containing } L \text{ random vectors as columns.} \quad (8)$$

Additionally, per prescriptions in [4], a number $2P$ of associated moments of the k dependent $L \times L$ matrix in (8) are computed and used to construct a generalized eigenvalue problem whose solution provides numerical values of the desired eigenvalues and eigenvectors. Here we determine the number $2P$ of moments used (which according to [19] should be such that PL is not smaller than the number of eigenvalues contained in the contour, counting multiplicities) on the basis of the SVD-based rank test introduced in [8]. For simple eigenvalues, such as appear most often for exterior scattering eigenvalues problems [20], it suffices [4] to choose $L = 1$ in the block SS method. Note that with this selection of the parameter L, the block SS algorithm is based on use of the scalarized resolvent (3)—exactly the same data utilized by Algorithm 1. The Beyn 1 method, in turn, utilizes the product in (8) with the matrix U^* replaced by the d-dimensional identity matrix. The number L of columns used in the Beyn 1 approach is selected on the basis of the aforementioned SVD-based rank test; in particular, the value L must at least equal the number of eigenvalues within the contour (counting multiplicities), and, to yield highly accurate results, it may need to be increased by a small number, perhaps as small as one or two (in accordance with the rank test), to account for the number of eigenvalues outside the contour but sufficiently close to it. For our comparisons we consider the problem of evaluation of eigenvalues of the Dirichlet problem in the exterior of the kite-shaped curve used for the experiments in Figure 2. In detail, using Algorithm 1 as well as the block SS and Beyn 1 methods we evaluate the eigenvalues contained within the circular contour $\mathcal{C}$ with center at $3 - 1.5i$ and radius 1, on the basis of equally spaced points along $\mathcal{C}$. The left panel in Figure 4 shows the eigenvalues within the curve $\mathcal{C}$ as computed by each method, while the corresponding right panel displays the error resulting from use of the various algorithms in the evaluation of the eigenvalue near $2.299 - 1.597i$ as a function of the number of points used along the contour $\mathcal{C}$, using the computation by Algorithm 1 with secant method as the reference solution. Errors resulting from use of the two different accuracy refinement
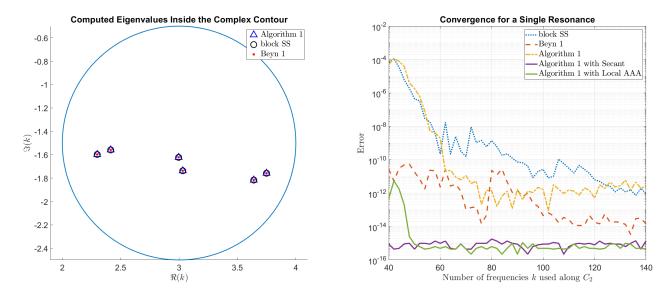
Figure 4: Comparison of Algorithm 1 to the block SS and Beyn 1 methods on the problem of evaluation of scattering poles outside the kite. Left panel: Eigenvalues computed by all three methods. Right panel: Errors computed by comparison with a secant method evaluation of the eigenvalue near $2.299 - 1.597i$. The curves labeled "with secant" were obtained by following the initial eigenvalue determination by four iterations of the secant method. For the curve labeled "with local AAA", four points were sampled on a circle of radius $1e-5$ around the initial AAA approximation of the pole together with a degree 1 rational approximant. To avoid underflow the maximum between the error and machine precision is plotted in all cases.

methods introduced in Section 5, namely, the secant method and the localized AAA approximation, are included in the figure as well.

Figure 4 shows that Algorithm 1 and the block SS method converge at similar rates, at least for a range of frequencies. While Beyn 1 converges faster than Algorithm 1 and block SS without local refinement, use of a local refinement technique on any of the three methods leads to similar convergence rates for the eigenvalues. Further, in situations where the LU factorization of the matrix discretization of the boundary integral equations is not available, such as may be the case in problems requiring large surface- or even volumetric-discretizations in 3D space, for which iterative solvers may need to be used, Algorithm 1 may prove more advantageous than Beyn 1—for which the need to incorporate a total of L matrix solves per frequency k along the contour, with values of L of the order of, say, a few tens, may become prohibitively expensive.

As indicated in Section 1, the fact that Algorithm 1 does not utilize a quadrature rule gives rise to a number of advantages in comparison with contour integration-based methods. In particular, the use of rational approximation results in geometric flexibility, such as, e.g., enabling the use of complex frequencies k that lie on a rectangular boundary in the complex plane, or even simple segments along the real axis, which in turn allows for simple adaptive algorithms such as the one introduced in Section 5 (Algorithm 2) without suffering a deterioration in convergence. While the use of such rectangular domains and associated adaptive algorithms could be envisioned in the context of contour-integration based methods, such a strategy may result in a significantly slower exponential rate of convergence than a circular contour would and, if the trapezoidal rule is used over the rectangular contour, where the contour integrand is not smooth, a somewhat erratic convergence may result, as illustrated in [19, Fig. 5.1(b)]. If Gauss-Lobatto quadrature is used on each side of a rectangle, in turn, the exponent that characterizes the exponential convergence rate is the approximately half of the one associated with the trapezoidal rule on a circular contour [19, Sec.
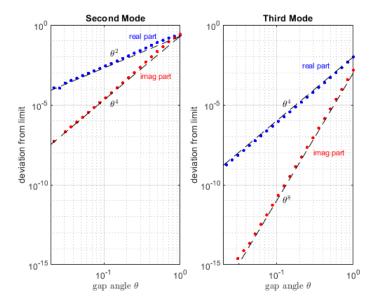
Figure 5: Convergence of $\Re(k)$ and $\Im(k)$ to their limiting values as the gap size θ shrinks to zero for the nearly degenerate open circle eigenfunctions displayed as the second and third images on the top row of Figure 3. For both modes the imaginary parts (decay rates) converge at twice the rates of the real parts (spatial frequencies), and both the rates for the real and imaginary parts for the third mode are twice those for the second mode. Note that for the third mode the approximate nodal line is aligned with the gap and thus results in a weaker coupling of interior and exterior fields and associated faster convergence.

5.2]. As a significant additional advantage, Algorithm 2 allows for the reuse of from previously used data points as the frequency mesh is refined with the goal of obtaining added accuracy for added accuracy—a strategy which cannot be used in the context of the Gauss-Lobatto quadrature. Finally, the applicability of the proposed algorithms on real segments instead of closed complex contours provides an important benefit e.g. for applications concerning real eigenvalues.

6.4 Dependence on Gap Size

With a tool in hand to compute scattering poles quickly and accurately, certain mathematical aspects of their behavior may be considered, such as, e.g., the convergence rate of a complex scattering pole associated with a open arc equal to the difference between a closed curve and a gap section, as the gap size shrinks to zero. As an example we consider the second and third modes shown in the top row of Figure 3, and associated eigenvalues (but for varying gap sizes θ) which, for small θ are approximately equal to the lowest double eigenvalue the closed unit circle ($\theta = 0$)—namely the first root ≈ 3.8317 of the Bessel function $J_1(x)$. Figure 5 demonstrates the convergence of $\Re(k)$ (the "spatial frequency") and $\Im(k)$ (the "decay rate") to their limiting values as θ shrinks to zero. The combined set of convergence computations for the two modes considered was completed in approximately four seconds on a single core of a present-day laptop computer.

The first image in Figure 5 shows that for the second mode in Figure 3, whose convergence rate we presume to correspond to generic gap-shrinking eigenvalue convergence behavior, the frequency converges to its limiting value ≈ 3.8317 at the rate $O(\theta^2)$ and the decay rate to its limiting value 0 at the rate $O(\theta^4)$. For the third mode in the figure, in turn, the rates double to $O(\theta^4)$ and $O(\theta^8)$. This is related to the

alignment of the nodal line of the eigenfunction with the gap, which reduces the field coupling between the interior and exterior regions of the open cavity. We are not aware of any theoretical or computational studies reporting on such convergence rates for scattering poles as opening gaps tend to zero.

The computations of Figs. 3 and 5 correspond to Dirichlet boundary conditions, and it is interesting to ask the same questions in the Neumann case. Here the first degenerate eigenvalue for the circle, associated with the first zero of the derivative of $J_1(r)$, is $1.84118\ldots$. Once again, introducing a gap in the boundary breaks the degeneracy. In separate computations (not shown) we have found that for the mode whose nodal line is aligned with the gap, the eigenvalue now converges at the rates θ^2 for the real part and θ^4 for the imaginary part, whereas for the more generic mode whose nodal line is orthogonal to the gap, the rates slow down dramatically to $1/|\log\theta|$ and $1/|\log\theta|^2$, respectively.

6.5 High-frequency Examples

Several higher-frequency examples are considered in what follows. To verify the accuracy of the proposed methods in high-frequency cases and in regions containing large numbers of eigenvalues we applied the real line version of algorithm 2 to obtain all 1244 distinct interior Laplace eigenvalues of the unit circle that are contained in the interval $[1, 100]$. The algorithm automatically obtained all 1244 eigenvalues with near machine accuracy in an average computational time of 1.09 seconds per eigenvalue in a single CPU core. This relatively slow figure is dominated by the higher eigenvalues; for example the average time per eigenvalue in the interval $[0, 25]$ is only about 0.08 seconds.
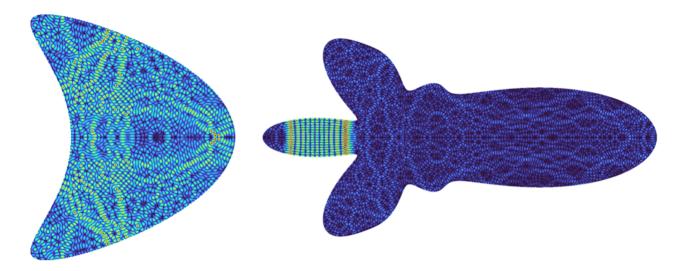

Figure 6: Left: Interior eigenfunction for the kite-shaped domain, with eigenvalue 100.1846738596. Right: Interior eigenfunction for the rocket-shaped domain, with eigenvalue 399.9730212127. All digits listed are believed correct on the basis of numerical convergence analyses.

Having verified our algorithm in the high-frequency regime, we subsequently applied the proposed methods to several high-frequency eigenvalue problems for interior and open-cavity domains. Figure 6 displays high-frequency interior eigenfunctions for kite-shaped and rocket-shaped cavities. The right panels in Figures 7 and 8, in turn, present eigenfunctions for circular and rocket-shaped open cavities, while the left panels of these figures present the solutions of problems of scattering by the same cavities under vertical upward-facing plane-wave illumination at frequencies equal to the real parts of the eigenvalues associated with the corresponding right panels. Clearly, the left panel scattering solutions bear a close resemblance with the eigenfuncions displayed in the right panels, suggesting that the open-cavity eigenfunctions can be excited by adequately oriented incident fields penetrating through the small apertures. All digits displayed
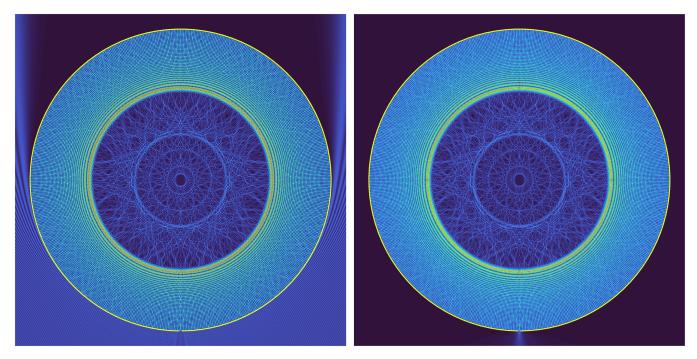
Figure 7: Comparison of the solution of the scattering problem with $k = 499.9073989141$ under vertical and upward plane-wave incidence (left) and the eigenfunction corresponding to the eigenvalue $499.9073989141 - 0.000779974959i$ (right) for an open circular cavity with aperture size $\pi/100$. All digits listed are believed correct on the basis of numerical convergence analyses.
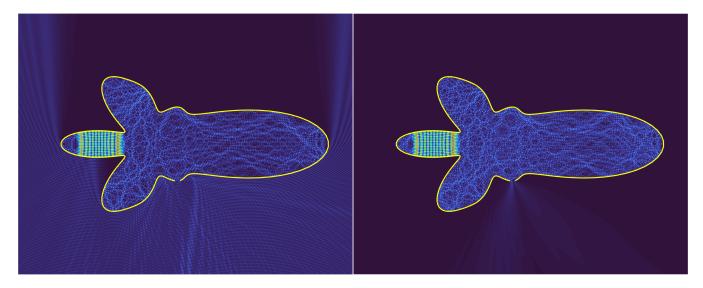

Figure 8: Comparison of the solution of the scattering problem with $k = 399.9694808817$ under vertical plane-wave incidence (left) and the eigenfunction corresponding to the eigenvalue $399.9694808817 - 0.00434495360i$ (right) for a rocket-like open cavity. The opening in the right curve is approximately equal to 0.6% of the curve length. All digits listed are believed correct on the basis of convergence analyses.

in the figure captions have been found to be correct by means of studies of convergence in both the discretization of the integral equations used and of the eigensearch algorithms utilized. For reference in Figures 7 and 8, the most refined solution used 16 points per wavelength which led to matrix discretizations of size 5000×5000 and 4000×4000 respectively and produced 13-digit accuracies.

7   Conclusions

This paper introduced a novel numerical algorithm for the evaluation of real and complex eigenvalues and eigenfunctions of general NEPs, including NEPs associated with Laplace eigenvalue and scattering-resonance problems for open and closed domains. Based on use of adaptive eigenvalue search methods based on AAA rational approximation combined with secant-method refinement, the algorithm produces highly accurate eigenpairs for challenging eigenproblems at both low and high frequencies. Comparisons with well-known contour-integration methods demonstrated a number of advantages of the proposed approach, including fast convergence and geometric flexibility. The latter characteristic is significant, in that it greatly facilitates use of the algorithm in a rectangular refinement-based adaptive strategy—resulting in automatic evaluation of all eigenvalues contained within a given region with near machine precision accuracy.

Acknowledgements

References

[1] Eldar Akhmetgaliyev and Oscar P. Bruno. Regularized integral formulation of mixed Dirichlet-Neumann problems. *Journal of Integral Equations and Applications*, 29:493–529, 2017.

[2] Eldar Akhmetgaliyev, Oscar P. Bruno, and Nilima Nigam. A boundary integral algorithm for the Laplace Dirichlet–Neumann mixed eigenvalue problem. *Journal of Computational Physics*, 298:1–28, 2015.

[3] Carlos J.S. Alves and Pedro R.S. Antunes. Wave scattering problems in exterior domains with the method of fundamental solutions. *Numerische Mathematik*, 156:1–20, 2024.

[4] Junko Asakura, Tetsuya Sakurai, Hiroto Tadano, Tsutomu Ikegami, and Kinji Kimura. A numerical method for nonlinear eigenvalue problems using contour integrals. *JSIAM Letters*, 1:52–55, 2009.

[5] C. E. Baum. The singularity expansion method. In Leopold B. Felsen, editor, *"Transient Electromagnetic Fields"*, pages 129–179. Springer Berlin Heidelberg, Berlin, Heidelberg, 1976.

[6] Timo Betcke, Nicholas J. Higham, Volker Mehrmann, Christian Schröder, and Françoise Tisseur. NLEVP: A collection of nonlinear eigenvalue problems. *ACM Transactions on Mathematical Software (TOMS)*, 39(2):1–28, 2013.

[7] Fridtjof Betz, Martin Hammerschmidt, Lin Zschiedrich, Sven Burger, and Felix Binkowski. Efficient rational approximation of optical response functions with the AAA algorithm. *Laser & Photonics Reviews*, 2024.

[8] Wolf-Jürgen Beyn. An integral method for solving nonlinear eigenvalue problems. *Linear Algebra and its Applications*, 436(10):3839–3863, 2012.

[9] Oscar P. Bruno and Stéphane K. Lintner. Second-kind integral solvers for TE and TM problems of diffraction by open arcs. *Radio Science*, 47(06):1–13, 2012.

[10] Oscar P. Bruno and Stéphane K. Lintner. A high-order integral solver for scalar problems of diffraction by screens and apertures in three-dimensional space. *Journal of Computational Physics*, 252:250–274, 2013.

[11] Dmitry A. Bykov and Leonid L. Doskolovich. Numerical methods for calculating poles of the scattering matrix with applications in grating theory. *Journal of Lightwave Technology*, 31(5):793–801, 2012.

[12] Younes Chahlaoui and Paul Van Dooren. A collection of benchmark examples for model reduction of linear time invariant dynamical systems. *EPrint 2008.22, Manchester Institute for Mathematical Sciences, University of Manchester, Manchester*, 2002.

[13] David L. Colton and Rainer Kress. *Integral Equation Methods in Scattering Theory*. John Wiley & Sons Inc., New York, 1983.

[14] David L. Colton and Rainer Kress. *Inverse acoustic and electromagnetic scattering theory, 4th Edition*. Springer, 2019.

[15] Tobin A. Driscoll, Nicholas Hale, and Lloyd N Trefethen. *Chebfun Guide*, 2014. www.chebfun.org.

[16] Mohamed El-Guide, Agnieszka Międlar, and Yousef Saad. A rational approximation method for solving acoustic nonlinear eigenvalue problems. *Engineering Analysis with Boundary Elements*, 111:44–54, 2020.

[17] Steven Elsworth and Stefan Güttel. Conversions between barycentric, RKFUN, and Newton representations of rational interpolants. *Linear Algebra and its Applications*, 576:246–257, 2019.

[18] Stefan Güttel, Gian Maria Negri Porzio, and Françoise Tisseur. Robust rational approximations of nonlinear eigenvalue problems. *SIAM Journal on Scientific Computing*, 44(4):A2439–A2463, 2022.

[19] Stefan Güttel and Françoise Tisseur. The nonlinear eigenvalue problem. *Acta Numerica*, 26:1–94, 2017.

[20] Frédéric Klopp and Maciej Zworski. Generic simplicity of resonances. *Helvetica Physica Acta*, 68(6):531–538, 1995.

[21] Alexandre Leblanc and Antoine Lavie. Solving acoustic nonlinear eigenvalue problems with a contour integral method. *Engineering Analysis with Boundary Elements*, 37(1):162–166, 2013.

[22] Pieter Lietaert, Karl Meerbergen, Javier Pérez, and Bart Vandereycken. Automatic rational approximation and linearization of nonlinear eigenvalue problems. *IMA Journal of Numerical Analysis*, 42(2):1087–1115, 2022.

[23] Stéphane K. Lintner and Oscar P. Bruno. A generalized Calderón formula for open-arc diffraction problems: theoretical considerations. *Proceedings of the Royal Society of Edinburgh*, 145(2):331–364, 2015.

[24] Yunyun Ma and Jiguang Sun. Computation of scattering poles using boundary integrals. *Applied Mathematics Letters*, 146:108792, 2023.

[25] William Charles Hector McLean. *Strongly elliptic systems and boundary integral equations*. Cambridge University Press, 2000.

[26] Volker Mehrmann and David Watkins. Polynomial eigenvalue problems with Hamiltonian structure. *Electronic Transactions on Numerical Analysis*, 13:106–118, 2002.

[27] Ryota Misawa, Kazuki Niino, and Naoshi Nishimura. Boundary integral equations for calculating complex eigenvalues of transmission problems. *SIAM Journal on Applied Mathematics*, 77(2):770–788, 2017.

[28] Yuji Nakatsukasa, Olivier Sète, and Lloyd N. Trefethen. The AAA algorithm for rational approximation. *SIAM Journal on Scientific Computing*, 40(3):A1494–A1522, 2018.

[29] Hermann W. Pommerenke, Johann D. Heller, Shahnam Gorgi Zadeh, and Ursula van Rienen. Computation of lossy higher order modes in complex SRF cavities using Beyn's and Newton's methods on reduced order models. *International Journal of Modern Physics A*, 34(36):1942037, 2019.

[30] Lothar Reichel and Qiang Ye. Breakdown-free GMRES for singular systems. *SIAM Journal on Matrix Analysis and Applications*, 26(4):1001–1021, 2005.

[31] Olaf Steinbach and Gerhard Unger. Convergence analysis of a Galerkin boundary element method for the Dirichlet Laplacian eigenvalue problem. *SIAM Journal on Numerical Analysis*, 50(2):710–728, 2012.

[32] Michael E. Taylor. *Partial differential equations. II.* Springer-Verlag, New York, 1996.

[33] Christian Wieners and Jiping Xin. Boundary element approximation for Maxwell's eigenvalue problem. *Mathematical Methods in the Applied Sciences*, 36(18):2524–2539, 2013.

[34] Lin Zhao and Alex Barnett. Robust and efficient solution of the drum problem via Nyström approximation of the Fredholm determinant. *SIAM Journal on Numerical Analysis*, 53(4):1984–2007, 2015.

[35] Frédéric Zolla, Gilles Renversez, André Nicolet, Boris Kuhlmey, Sebastien R.L. Guenneau, and Didier Felbacq. *Foundations of photonic crystal fibres*. World Scientific, 2005.